JOURNAL OF SPACECRAFT AND ROCKETS
Vol. 33, No. 5, September–October 1996

Visual Utility for the Localization of Corona-Accelerated Nuclei

J. Spagnuolo Jr.,* Cecilia Cheng,† U. M. Schwuttke,‡ and Felipe Hervias†
Jet Propulsion Laboratory, California Institute of Technology, Pasadena, California 91109-8099

The proton prediction system developed by Smart and Shea (Smart, D. F., and Shea, M. A., "PPS76—A Computerized 'Event Mode' Solar Proton Forecasting Technique," *Solar Terrestrial Prediction Proceedings*, edited by R. F. Donnelly, Vol. 1, National Oceanic and Atmospheric Administration/Environmental Research Lab., U.S. Dept. of Commerce, 1979, pp. 406–423) provides the approximate magnitude of the fluxes of solar-flare-ejected protons in the vicinity of the Earth. A system is described that extends Smart and Shea's work in that it predicts fluxes of such protons at arbitrary points of the inner heliosphere near the plane of the solar equator. It has interactive graphical components that enhance the user's overall perception of a flare's effects upon the solar system while also providing precise user-requested data. The flux predictions of the system agree well with proton fluxes as measured by various spacecraft. Results are given. A database of flare events is maintained and can be used for a retroactive analysis when it is desired to know the magnitudes of potential proton fluxes due to a previous flare.

Nomenclature

a	= distance from the sun to a point under discussion divided by a quantity discussed in Eqs. (15–22)
$d(x, y)$	= distance from a point or body x to a point or body y, km
$r_\odot$	= radius of the sun
(x_b, y_b)	= coordinates of a point b with respect to a heliocentric coordinate system whose x–y plane passes through the solar equator
ε	= center of the Earth
ε-point	= point contained in the intersection of ε-sun plane and solar equator that is closest to Earth
ε-sun plane	= plane containing the center of the Earth and the north and south poles of the sun
λ_F	= heliocentric latitude of the solar flare F, rad
ξ	= angle used to form the spiral shape as discussed in Eqs. (15–22), rad
τ	= an arbitrary point in space
τ_i	= a point in space at position i
τ-point	= point in the intersection of τ-sun plane and solar equator that is closest to τ
τ-sun plane	= plane containing an arbitrary point in space τ and the north and south poles of the sun
ϕ_A	= Archimedean angle, rad
ϕ_F	= heliocentric longitude of the solar flare F with respect to Earth, rad
ϕ_L	= vertical angle between a line L passing through the sun's center and the solar equator, rad
$\phi_{\varepsilon,\tau}$	= angle between the ε point and the τ point along the solar equator, rad

Introduction

THERE is considerable controversy as to whether flares are the sole producers of energetic protons or whether coronal mass ejections play a central role. We note that the system described in this paper is presently capable of computing flux predictions only for protons associated with solar-flare activity. The techniques used in this paper do not permit the inclusion of a shock-associated particle increase such as is often present at the passage of an interplanetary shock. Therefore, even if not explicitly stated, all proton fluxes discussed in this paper will be those associated with flares.

Solar-flare-associated phenomena can cause a variety of difficulties in spacecraft mission operations.[1] Detailed knowledge of the intensity of the proton fluxes over time from an observed solar flare can provide information to mission personnel that would enable them to minimize the effect of flares on operations. Further, if some aspect of mission operations exhibited unexpected behavior in the past, it would be useful to rule out or demonstrate the possibility that solar-flare-associated phenomena might have been the source of the problem. Such a retroactive analysis has already been done with respect to Mars Observer[2] and Topex.[3]

Much work has been done on determining the criteria for predicting the impact of solar-flare-ejected protons upon the Earth.[4] Smart and Shea[5,6] and Heckman et al.[7] have devised models that predict the fluxes at Earth on the basis of certain electromagnetic indicators sent out by the flares. The Smart–Shea and Heckman models yield flux data for Earth that are generally within an order of magnitude of the real flux values.

It was desired to determine whether the underlying ideas of any of these existing systems could be generalized to predict proton fluxes for points of the solar system other than Earth. It was also desired to add appropriate graphics that would enhance the user's overall perception of the solar flare's effects upon the solar system while providing, at any time, precise and accurate flux data. The solar-flare tool developed from these specifications is called the visual utility for the localization of corona-accelerated nuclei (VULCAN) and is named after the Roman god of fire. The basis for VULCAN is the Smart–Shea model,[5,6] referred to as PPS86. Smart and Shea described how to extend their model to the inner heliosphere near the plane of the solar equator[8,9] and were readily available for discussions on the scientific as well as practical aspects of their work. These reasons, together with the long documentation and implementation history characterizing PPS86, made it a good choice for the basis of VULCAN.

VULCAN relies on 1–8-Å peak x-ray data from the National Oceanographic and Atmospheric Administration (NOAA) in Boulder, Colorado, for indication of solar-flare activity. The peak flux, the time of detection, and the latitude and longitude associated with the flare are also sent. Fluxes resulting from proton producing locations outside of the visible 180-deg area for Earth are not computed by VULCAN, as NOAA is not able to acquire the requisite x-ray data. Required planetary data are provided by the SPICE[10] system. The SPICE system provides ephemeris data and associated software that accurately computes the positions of the sun, planets, spacecraft, and other celestial bodies of interest over specified periods of time. Advantages of using VULCAN include improved

Received April 20, 1995; revision received March 2, 1996; accepted for publication March 2, 1996.

*Senior Member, Technical Staff, Information Systems Development and Operations Division.
†Member, Technical Staff, Information Systems Development and Operations Division.
‡Group Leader, Advanced Multimission Software Technology Group, Information Systems Development and Operations Division.

efficiency in solving ground-link and instrumentation failure problems, specific options relating to the delay of communications between ground stations until peak disturbances have subsided, and possible opportunities for conducting science observations.

Comparisons of VULCAN's flux computations vs measured proton fluxes for spacecraft in the inner heliosphere near the plane of the solar equator are presented in the last section of the paper. For points outside this region, the validity of the VULCAN software is less certain. However, VULCAN has the capability of incorporating arbitrary trajectories into its graphics and computational modules to derive a prediction of fluxes at points away from the solar equator outside the inner heliosphere, thus enabling future experimentation with the program to determine the limits of its accuracy.

Even though Smart and Shea produced specifications for extending their proton prediction model, other techniques having a geometric and analytic nature had to be developed to facilitate the merging of these specifications with their already existing theory to produce VULCAN. Aside from the discussions of the graphics displays, the presentation of certain of these mathematical considerations characterizes what follows.

Flare-Angle Determination

Background

Data required to run VULCAN are obtained from the Space Environment Laboratory of NOAA in Boulder, Colorado. In addition to parameters relating to the time of the flare and its associated x-ray data, the latitude and longitude of the flare with respect to the Earth are obtained. The exact meaning of the phrase latitude and longitude with respect to x will be given in the following discussion. The purpose of the flare extrapolation algorithm is to use the latitude and longitude of a flare with respect to Earth to determine the location of the flare with respect to an arbitrary point in space at which we wish to compute the fluxes.

Geometry

To describe the flare-angle extrapolation algorithm, we first discuss certain geometrical aspects of the problem. The spatiality of the ε–sun plane, the τ–sun plane, the ε point, and the τ point are illustrated in Fig. 1a. Here, the four asterisks represent the north and south poles of the sun, ε, and τ. The dashed curved lines represent the intersections of each of the planes with the sun's surface. The angle $\phi_{\varepsilon,\tau}$ is shown as well. Figure 1b presents a top view of Fig. 1a. Since the familiar generalized form of the Pythagorean theorem is used to derive $\cos\phi_{\varepsilon,\tau}$, we have $0 \leq \phi_{\varepsilon,\tau} \leq \pi$. An appropriate sign will be given to the angle $\phi_{\varepsilon,\tau}$ based upon considerations presented in the following discussion.

As mentioned earlier, the latitude and longitude of the flare are computed and sent to VULCAN by NOAA at Boulder, Colorado. Latitude is measured in the intervals $[0, \pi/2]$ and $[0, -\pi/2]$ going from the solar equator to north pole and south pole respectively. As labeled in Fig. 1b, positive longitude (from the earth's perspective) is measured counterclockwise (from the vantage point of the north pole) on the solar equator in the interval $[0, \pi]$, where 0 is the ε point. Negative longitude is measured clockwise in the interval $[0, -\pi]$. The longitude of a flare as sent by NOAA is approximately in the interval $[-\pi/2, \pi/2]$, since it has to be seen by Earth. The longitude of a flare with respect to an arbitrary point τ in space is subject to the same interval conventions as mentioned above except that the flare longitude is measured in relation to τ. The theory underlying VULCAN is such that if it is desired to compute the flux at a point in space, then the latitude and longitude of the flare with respect to that point (measured as described above) must be used in the computation. If L is a line drawn from the sun center to the point in space, then the latitude of the flare with respect to the point is easily given by $\lambda_F - \phi_L$. However, the longitude of the flare from NOAA is given with respect to the ε-point and not with respect to a fixed location on the sun (as latitude is with respect to the solar equator). Therefore, the longitude of the flare has to be adjusted in a more complicated fashion to compute the flux for points other than at Earth. The purpose of the flare-angle extrapolation algorithm is to compute this adjusted longitude given the longitude of the flare as sent by NOAA. To derive the proper longitude to compute the flux at a point τ, we must use the flare longitude with respect to Earth and the longitudinal angle $\phi_{\varepsilon,\tau}$ that is as shown in Fig. 1b.

A demonstration of what is involved in this computation involves a consultation of Fig. 2. The quantities $\phi_{\varepsilon,\tau_1}$ and $\phi_{\varepsilon,\tau_2}$ are the angles between the Earth and the points at positions 1 and 2, respectively. The positions of the planets are computed with respect to an x–y–z coordinate system where the x–y plane is the plane of the solar equator. The quadrants are numbered as indicated. In general, to determine the longitude of a flare with respect to a point in space, the algorithm first computes the magnitude of the longitudinal angle between the ε point and the τ point in space as defined earlier. By examining the flare angle, the flare extrapolation algorithm does a case-by-case analysis based on the quadrants the planets are in. The quadrants are based upon the ε point and the τ point as discussed earlier. Using these cases, the program determines whether to add plus or minus the angle between the Earth and τ to the already known flare angle ϕ_F (given with respect to Earth), to obtain the angle between τ and the flare. For example, if the Earth is in quadrant I

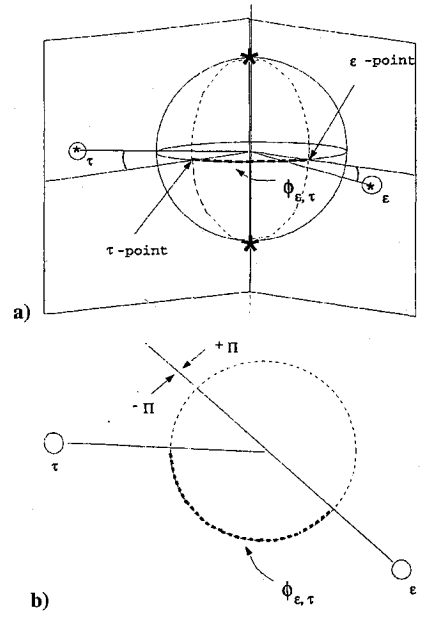

Fig. 1 Earth and τ planes: a) side perspective and b) top perspective of ε–sun plane and τ–sun plane.

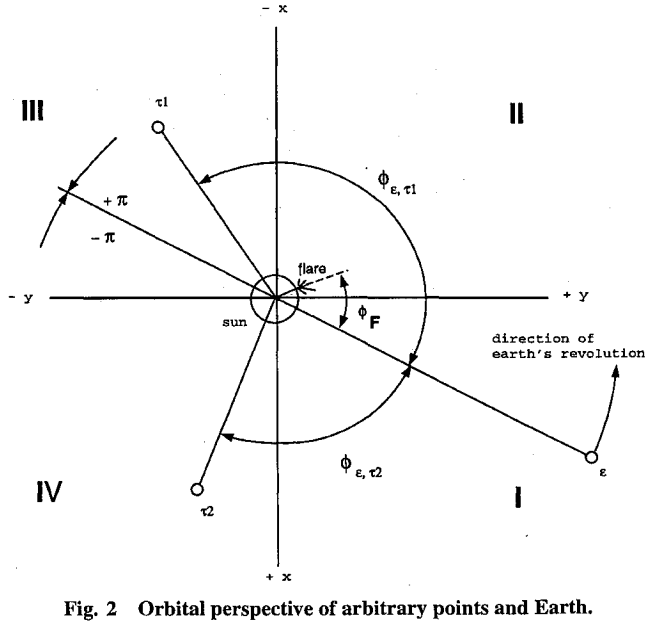

Fig. 2 Orbital perspective of arbitrary points and Earth.

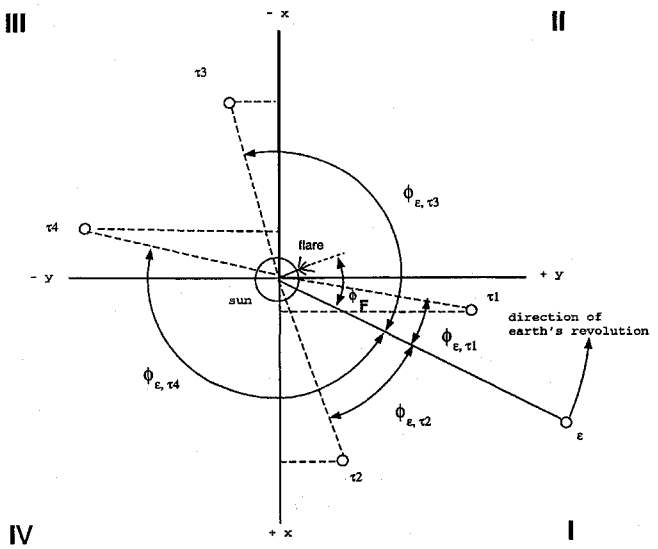

Fig. 3 Some positions requiring arctangent treatment.

and if τ is in quadrant III, a sample orientation of which is shown in Fig. 2, then the angle between the target at position 1, τ_1, and the flare is $\phi_F - \phi_{\varepsilon,\tau_1}$. If the Earth is in quadrant 1 and τ is in quadrant IV, then the angle between the flare and τ_2 is $\phi_F + \phi_{\varepsilon,\tau_2}$. When the angle falls outside the intervals $[0, \pi]$ and $[0, -\pi]$ mentioned earlier, the program will adjust it so that it is within these intervals. We discuss this in what follows.

Knowing which quadrants the Earth and target are in is generally not sufficient for determining $\phi_{\varepsilon,\tau}$. If the Earth and target are in the same quadrants or are in opposite quadrants (I and III or II and IV), it is not clear whether to add $\phi_{\varepsilon,\tau}$ to or subtract it from ϕ_F to determine the longitude of the flare with respect to the point τ. In these cases, the arctangent function is used to determine the relative positions of flare and target. For example, in Fig. 3, a target in quadrant III could be in position 3 or 4. In position 3, the angle between the flare and τ is $\phi_F - \phi_{\varepsilon,\tau_3}$. However, if τ is at position 4, the angle between the target and the flare is $\phi_F + \phi_{\varepsilon,\tau_4}$. Note that this angle falls outside the prescribed longitudinal intervals $[0, \pi]$, $[0, -\pi]$. In this case, the algorithm adds -2π to its value so that it does fall in one of the prescribed intervals. If a target is in the same quadrant as the Earth, ambiguities arise as well. In position 1, the angle between the flare and τ is $\phi_F - \phi_{\varepsilon,\tau_1}$, whereas in position 2 the angle is $\phi_F + \phi_{\varepsilon,\tau_2}$. In fact, if τ and ε are in quadrant I, then whether $\phi_{\varepsilon,\tau}$ is added to or subtracted from ϕ_F depends upon whether τ's position is clockwise or counterclockwise to the ε–sun plane. Also, if ε is in quadrant I and τ is in quadrant III, then whether $\phi_{\varepsilon,\tau}$ is added to or subtracted from ϕ_F depends on whether τ's position is counterclockwise or clockwise to the extension of the ε–sun plane into quadrant III. We now show how these ambiguities are resolved by use of the arctangent function. In what follows we assume that $(x_\varepsilon, y_\varepsilon)$ are the coordinates of Earth and $(x_{\tau\zeta}, y_{\tau\zeta})$ are the coordinates of τ at position ζ for $1 \leq \zeta \leq 4$. It can be determined that in quadrant I $\arctan(y_{\tau_1}/x_{\tau_1}) > \arctan(y_\varepsilon/x_\varepsilon)$. We can use this information to conclude that $\phi_{\varepsilon,\tau_1}$ can be subtracted from ϕ_F to obtain the correct angular distance between τ and the flare when τ is in position 1. Further, based upon the fact that $\arctan(y_{\tau_2}/x_{\tau_2}) < \arctan(y_\varepsilon/x_\varepsilon)$, the algorithm adds the angle $\phi_{\varepsilon,\tau_2}$ to ϕ_F when τ is in position 2 to determine the angle between the flare and τ_2. Using similar reasoning for the third quadrant, the fact that $\arctan(y_{\tau_3}/x_{\tau_3}) < \arctan(y_\varepsilon/x_\varepsilon)$ can be used to determine that the angle between the target at position 3 and the flare is $\phi_F - \phi_{\varepsilon,\tau_3}$. Also, since $\arctan(y_{\tau_4}/x_{\tau_4}) > \arctan(y_\varepsilon/x_\varepsilon)$, the angle between the flare and τ at position 4 is $\phi_F + \phi_{\varepsilon,\tau_4}$. We note that the geometrical relations displayed in the figures are only examples used to illustrate techniques that are used in an extended and modified form throughout the algorithm and represent only a subset of what has to be considered, to determine the angle between τ and F given more general initial configurations of ε, τ, and F.

Analysis

Background

In the last section, we gave an overall view of the spatial orientation between points that were determined by the ε–sun plane and various τ–sun planes intersecting the solar equator. In this section, we determine the coordinates of an arbitrary 'x'-point given the coordinates of an arbitrary point x. From this, we can then find a general form for the distances between the ε point and the sun center, between a τ point and the sun's center, and between the ε point and the τ point. This enables us to determine the angle $\phi_{\varepsilon,\tau}$ between the Earth and τ using the generalized Pythagorean theorem. We assume that the Cartesian plane in which all computations are done has as its origin the center of the sun with the $+z$ and $-z$ axes passing, respectively, through the north and south poles of the sun.

Formulation

Given that τ is an arbitrary point in space, possibly representing Earth or any other planet, spacecraft, or object in the solar system, we first determine the equation of the τ–sun plane. In our chosen coordinate system, the origin, north pole, and projection of the center of τ on the x–y Cartesian plane are all in the τ plane. These points are denoted by $(0, 0, 0)$, $(0, 0, z_n)$, and $(x_p, y_p, 0)$, respectively. From this, we deduce that the equation of the τ plane satisfies

$$Ax_p + By_p = 0 \tag{1}$$

If both x_p and y_p are 0, then τ is at the north or south pole and the Archimedean solar transport model does not apply. We thus assume that both are not simultaneously equal to 0. If x_p is 0 and y_p is not 0, then $\tau = (0, vr_\odot)$, where v is the sign of y_p. If y_p is 0 and x_p is not 0, then $\tau = (vr_\odot, 0)$, where v is the sign of x_p. The following analysis assumes therefore that neither x_p nor y_p is equal to 0. Since this assumption in turn implies that $A = 0$ if and only if $B = 0$, we therefore assume also that A and B are both unequal to 0 in the analysis which follows.

From the preceding paragraph, we can normalize the coefficient of x and obtain

$$x - (x_p/y_p)y = 0 \tag{2}$$

as the equation of the τ plane. Since the τ point intersects the solar equator, we have

$$x = (x_p/y_p)y = (x_p/y_p)\left(\pm\sqrt{r_\odot^2 - x^2}\right) \tag{3}$$

resulting in

$$x^2 = (x_p/y_p)^2 r_\odot^2 - (x_p/y_p)^2 x^2 \tag{4}$$

Thus, the possible coordinates for the τ point are

$$x = \pm\frac{r_\odot(x_p/y_p)}{\sqrt{1 + (x_p/y_p)^2}} \tag{5}$$

and

$$y = \pm\frac{r_\odot}{\sqrt{1 + (x_p/y_p)^2}} \tag{6}$$

where the plus-or-minus signs are due to the fact that the τ plane intersects the solar equator in two places. Note that there are only two pairs of coordinates (as opposed to four) because from Eq. (2) the positive root is used for y if and only if the positive root is used for x. We next compute the distance from $(x_p, y_p, 0)$ to each set of coordinates $(x_+, y_+, 0)$ and $(x_-, y_-, 0)$, where the former denotes the positive roots of Eqs. (5) and (6), and the latter the negative roots. We then choose the coordinates that represent the point that is closer to $(x_p, y_p, 0)$, since the distance from $(x_p, y_p, 0)$ to the τ-point is always less than the distance from $(x_p, y_p, 0)$ to the point directly opposite the τ-point on the solar equator. In mathematical terms, if we define

$$d_i = \sqrt{\left(x_p + (-1)^i \sqrt{\frac{r_\odot^2}{(x_p/y_p)^2 + 1}} \frac{x_p}{y_p}\right)^2 + \left(y_p + (-1)^i \sqrt{\frac{r_\odot^2}{(x_p/y_p)^2 + 1}}\right)^2} \tag{7}$$

then

$$\tau \text{ point} = \begin{cases} (x_-, y_-) & \text{if} \quad d_0 = \min\{d_0, d_1\} \\ (x_+, y_+) & \text{if} \quad d_1 = \min\{d_0, d_1\} \end{cases} \tag{8}$$

Equations (7) and (8) could have been replaced by a procedure that compared coordinate signs between (x_-, y_-) and (x_p, y_p) and between (x_+, y_+) and (x_p, y_p); however, we felt that the mathematical approach was cleaner than a case-by-case analysis.

Graphics

Archimedean Spiral

The Archimedean angle with respect to a point τ is defined as the angular distance that the sun rotates in the time it takes for a

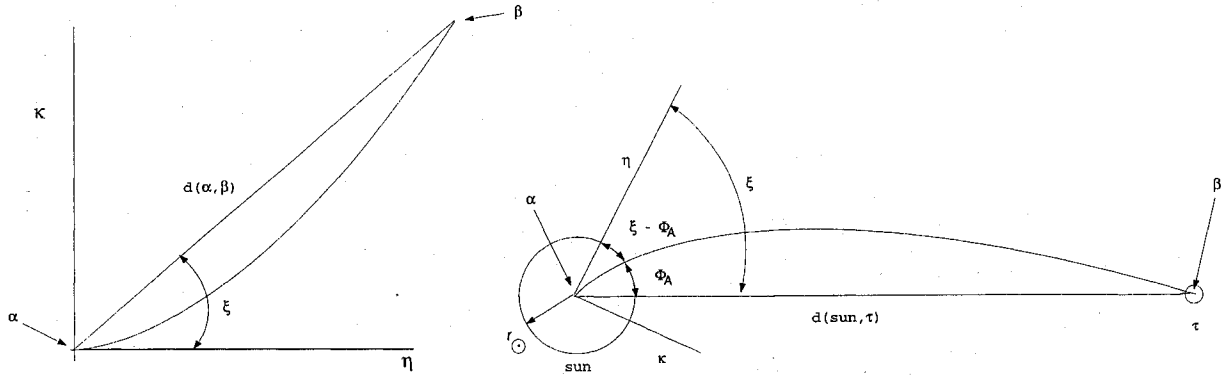

a) Graph of $\rho = [d(\alpha, \beta)/\xi]\theta$ for $0 \leq \theta \leq \xi$ b) ρ curve embedded in sun–τ relationship

Fig. 4 Archimedean–spiral analysis.

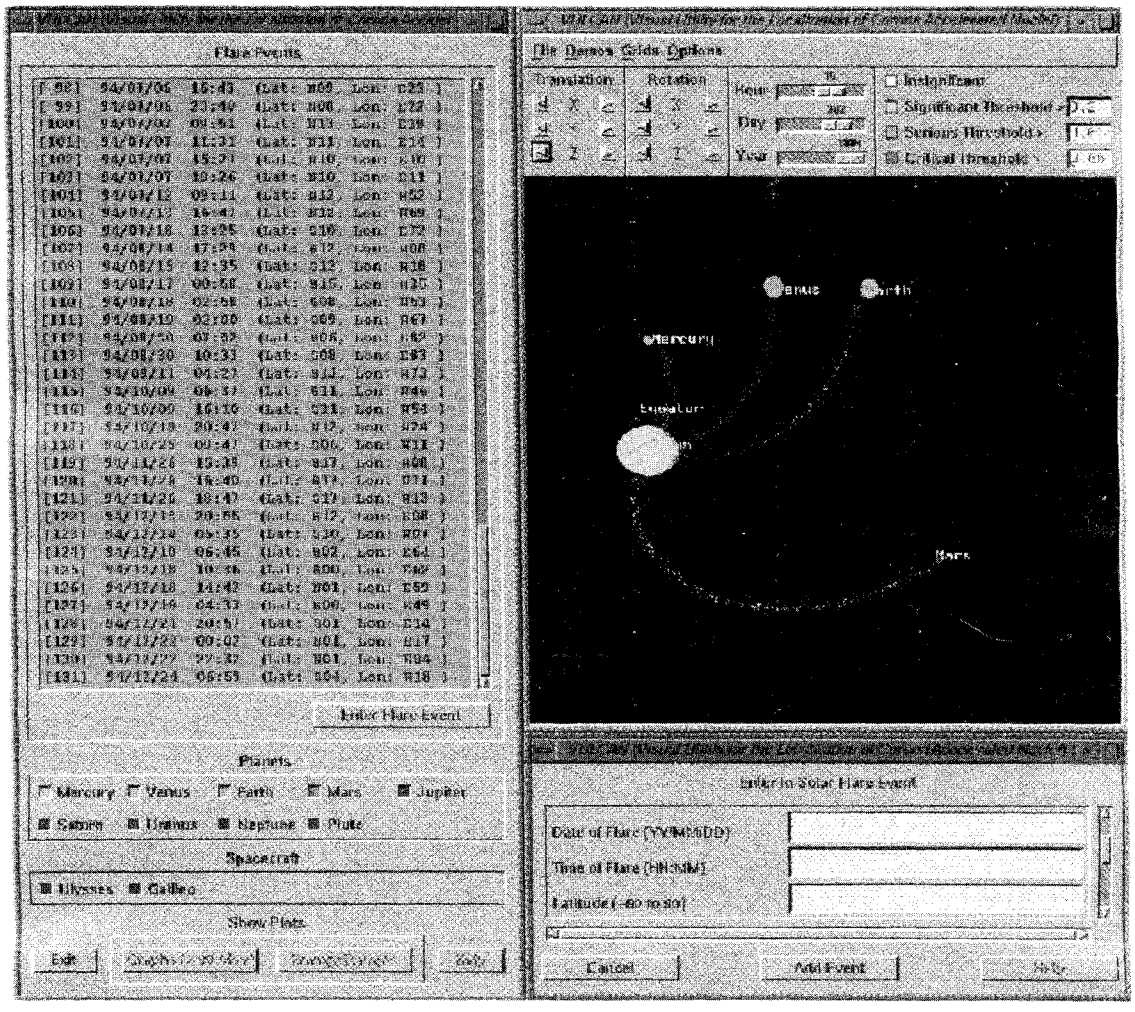

Fig. 5 Intuitive view of flux data.

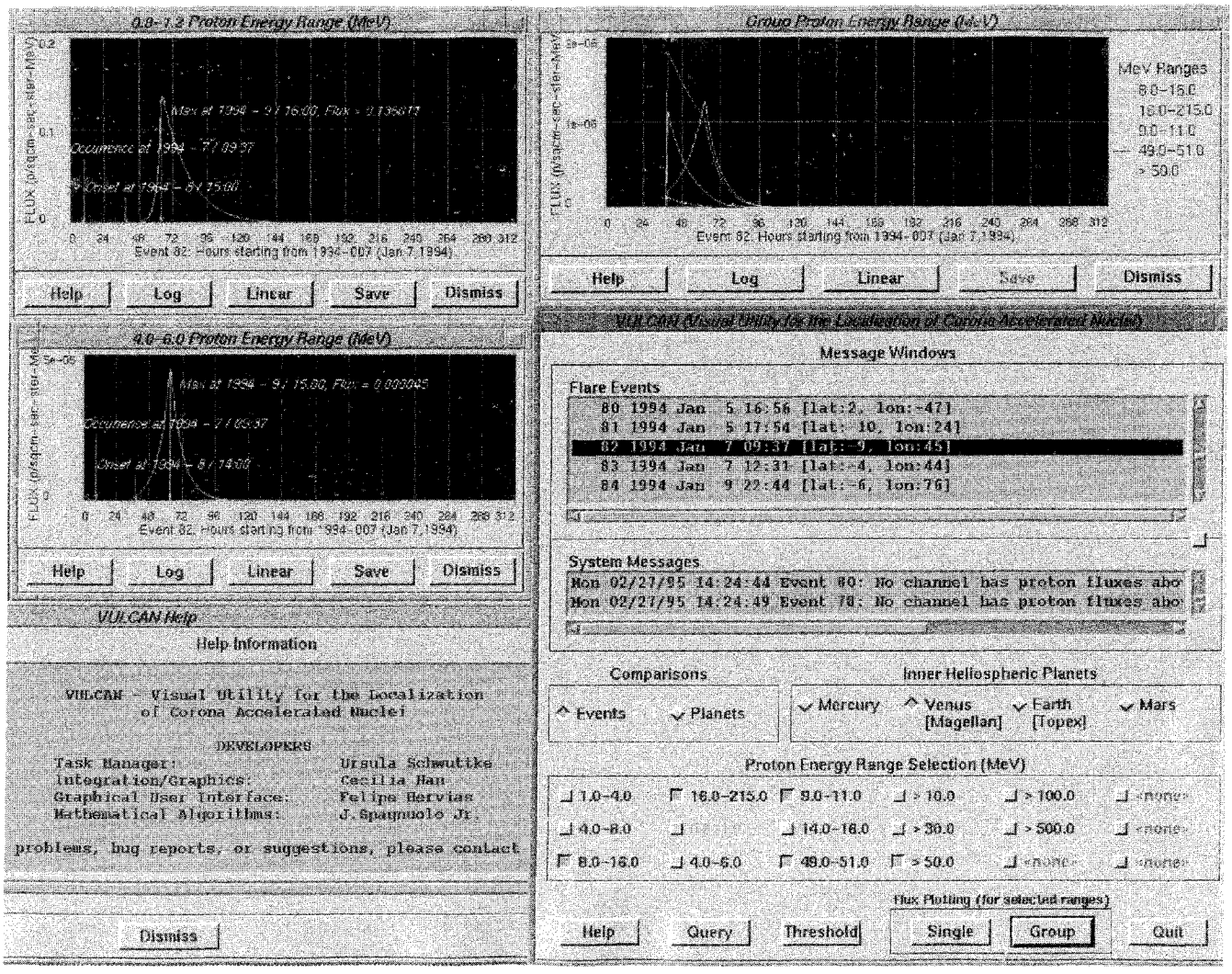

Fig. 6 Analytic view of flux data.

particle to go from the sun to τ, assuming it leaves the sun in a radial path. This is also expressed by the formula $\phi_A = \omega_s r/V$, where ω_s is the angular rotation rate of the sun, r is the distance from the sun to the point, and V is the speed of the particle. For any point in the inner heliosphere near the plane of the solar equator, present models of solar-particle transport assume that the protons travel along a pathway in the form of an Archimedean or Parker Spiral[4,11] given by

$$\rho = a\theta, \qquad 0 \le \theta \le \xi \tag{9}$$

where ξ (which will be more fully discussed below) is related to ϕ_A with respect to that point and a is the distance from the sun to the point in question divided by ξ. In what follows, we discuss how to construct the Archimedean spiral graphically. For purposes of exposition, we will assume that τ is in the plane of the solar equator, since if it is not, we can imagine rotating it into the solar equator and then going through the spiral-construction reasoning that will be presented in the following discussion. The computationally visualized spiral for τ in its original position is then obtained by returning the rotated point τ to its original position with the constructed spiral attached, keeping shape as it was formed with respect to the plane of the solar equator.

The graph of the above function has the approximate form shown in Fig. 4a. The astronomical interpretation of this graph is realized by embedding it in the sun–τ spatiality as shown in Fig. 4b. The correspondence of the labels α, β, η, and κ in Figs. 4a and 4b indicates that the spiral shape in Fig. 4a was flipped and rotated to obtain the orientation displayed in Fig. 4b. The view in Fig. 4b is from a northerly perspective. Here $d(\text{sun}, \tau)$ is the length of the line connecting the sun to the point τ. The angle that the graph makes with the line connecting the sun with τ is interpreted as being ϕ_A. The graphical creation of the shape of the Archimedean spiral thus has two requirements: 1) it must be of the form given by Eq. (9), and 2) it must be such that when one end is placed at the sun's center and the other at τ, as shown in Fig. 4b, its intersection with the solar equator is at longitude ϕ_A , the given calculated Archimedean angle for the point τ.

Both 1) and 2) require the determination of the angle ξ. To this end, we note that, in view of both diagrams in Fig. 4 and the definition of a,

$$r_\odot = a(\xi - \phi_A) \tag{10}$$

and

$$d(\odot, \tau) = a\xi \tag{11}$$

Eliminating a gives

$$\frac{r_\odot}{\xi - \phi_A} = \frac{d(\odot, \tau)}{\xi} \tag{12}$$

resulting in

$$\xi = \frac{\phi_A}{1 - [r_\odot / d(\odot, \tau)]} \tag{13}$$

The magnitude of the difference of the two angles ξ and ϕ_A is therefore

$$\xi - \phi_A = \frac{\phi_A}{[d(\odot, \tau)/r_\odot] - 1} \tag{14}$$

Table 1

Event	Spacecraft	Particle energy, MeV	Flux	
			Measured	Computed
Aug. 2, 1972, 7:58 PM, lat 14 lon −28	Pioneer 9	>14	~900	279
Nov. 22, 1977, 9:46 AM, lat 24 lon 38	Voyager I	>10	~23	18.7
March 6, 1989, 1:13 PM, lat 35 lon −70	Phobos II	0.9–1.2	~9000	7.4×10^4
March 17, 1989, 5:20 PM, lat 31 lon 60	Phobos II	0.9–1.2	~720	584

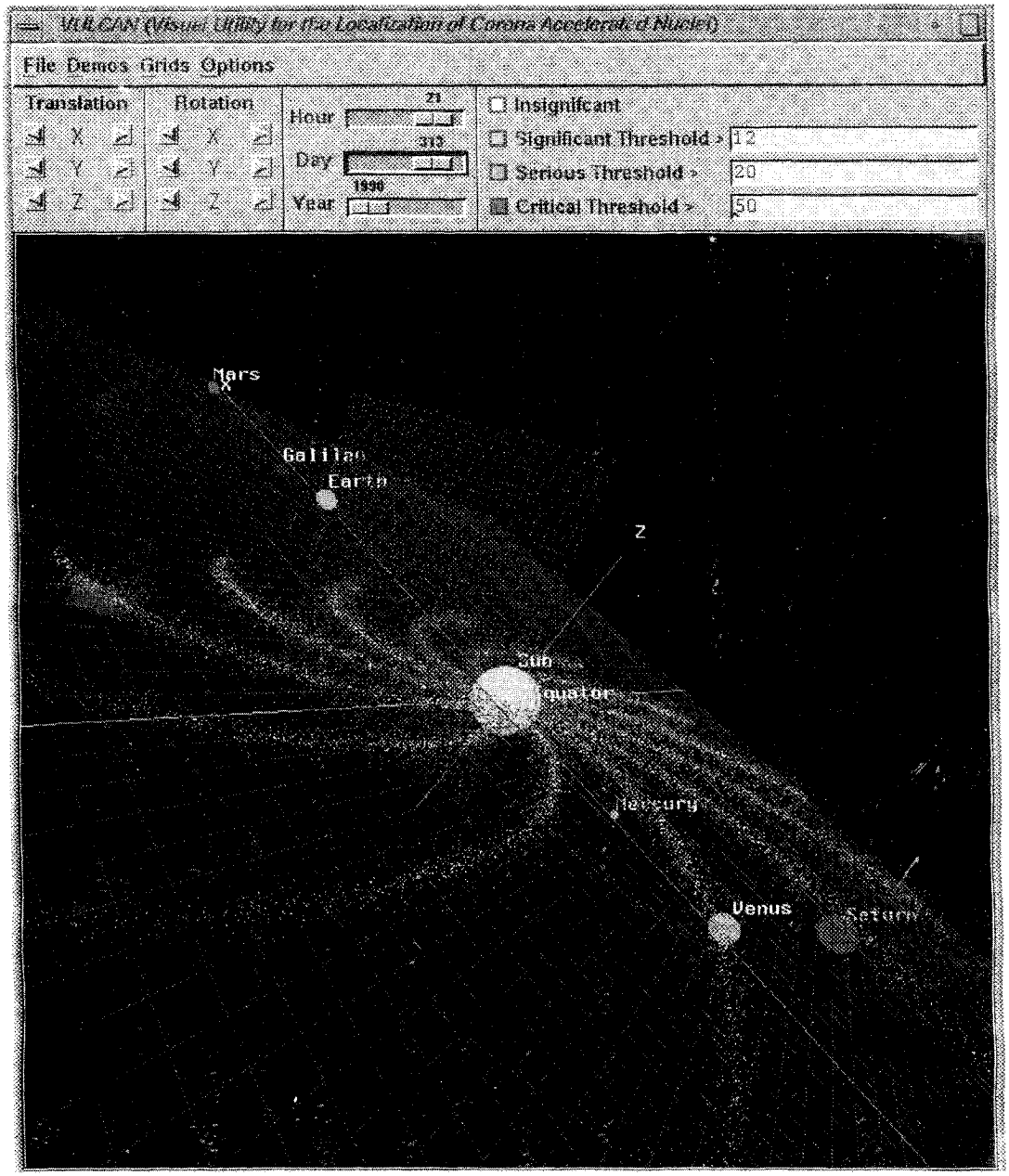

Fig. 7 Perspective of the heliosphere.

indicating that for computations where real astronomical parameters are used,

$$\frac{d(\odot, \tau)}{r_\odot} \gg 0 \quad \longrightarrow \quad \xi \approx \phi_A \tag{15}$$

However, for purposes of graphical presentation, the relative magnitudes of distances and planet sizes are considerably different from those used in realistic computations characterizing solar physics. To facilitate display, the ratio of the distance between the sun and τ to the radius of the sun may be much smaller than in reality, implying that the difference between ϕ_A and ξ is not very small, thus justifying the above treatment.

Interactive Visual Configurations

There are essentially two ways that VULCAN has of presenting solar-flare data to the user. The first is intuitive. The second is analytical. Upon reception of solar-flare data, the former gives an immediate overall view of the solar-flux conditions at various points of the inner heliosphere, whereas the latter allows the user to obtain more precise flux-related data at an arbitrary point. These two modes of computational presentation complement one another in the sense that the point the user chooses to analyze using the perspective afforded by the second mode is generally influenced by the overall view of the flux intensities displayed by the first mode.

Figure 5 shows the windows for the intuitive treatment of the solar system. The leftmost window has a listing of the received flare events from Boulder. In the rightmost window, the color of each Archimedean spiral indicates the intensity of the protons going from sun to planet. Figure 6 presents more detailed flux information relating to flare events. Here flux-vs-time graphs are displayed for various user-selected planets and proton energy ranges. Finally, Fig. 7 displays the continuous movement of particles in time throughout the solar system. A capability for displaying the various orbital planes exists as well. The solar equator and the ε–sun plane are displayed.

Comparisons with Real Data

Computed maximal values of the flux as compared with those measured by actual spacecraft at varying positions with respect to the sun are shown in Table 1. Spacecraft distances from the sun ranged from 0.77 to 1.52 AU. The differential flux values are measured in protons/cm^2 · s · sr · MeV, and correspondingly the integral flux is measured in protons/cm^2 · s · sr. The actual flare angle with respect to the Earth–sun line was given by NOAA at Boulder. The flare extrapolation algorithm used the spacecraft trajectory to compute the ESP angle, subsequently deriving the angle between the spacecraft and flare. Table 1 represents all cases in which we were able to obtain sufficient flare and spacecraft data for comparison.[9,12–14] The computed values are in accordance with the expected accuracy of the Smart–Shea model.

Conclusions

We have developed a system that directly receives data from NOAA via modem and uses ephemeris data to predict the effects of solar flares on the planets and spacecraft (near the solar equator) of the inner heliosphere. Experimentation with the model's underlying predictive capability at other points of the solar system is possible also, although the accuracy of the computed fluxes is not guaranteed in this region. The system allows as input user-constructed flare events or those on record as sent by NOAA to determine what fluxes will result, be they in the past or in the future. Graphical user interfaces together with manipulable views of the solar system and color coding of proton flux paths facilitate experimentation with interdependent parameters. This allows determination of how an alteration of their values causes variations on the computed distribution over time of solar particles at various points throughout the solar system. The accuracy of the model has been demonstrated.

Acknowledgments

The authors would like to thank M. Shea and D. Smart for their scientific collaboration. We would also like to thank Neil Toy, Harry Woo, Ed Ng, Guy Spitale, Alan Quan, Robert Angelino, Jim Gersbach, and Mike de Gyurky for their technical support and managerial assistance during the course of this work. The system can be obtained by contacting any of the authors of this paper via e-mail at ⟨author_name⟩@ jpl.nasa.gov or contacting the Information Systems Development and Operations Division at the Jet Propulsion Laboratory.

References

[1]Robinson, P. A., Jr., "The Effects of High Energy Particles on Planetary Missions," *Proceedings of the JPL Workshop in the Interplanetary Charged Particle Environment*, edited by J. Feynman and S. Gabriel, NASA JPL Publication 88-28, 1988, pp. 39–46.

[2]Spitale, G. C., "Solar Event Environment at Mars at the Time of Loss of Communications with Mars Observer," Jet Propulsion Lab., JPL Interoffice Memorandum 5215-93-267, California Inst. of Technology, Pasadena, CA, Oct. 1993.

[3]Richter, R., and Spagnuolo, J., Jr., "Energetic Solar Particle Activity During the Time of Astra 1-B Failure," Jet Propulsion Lab., JPL Interoffice Memorandum 3544-TOP-94-001, California Inst. of Technology, Pasadena, CA, Jan. 1994.

[4]Cliver, E. W., Secan, J. A., Beard, E. D., and Manley, J.A., "Prediction of Solar Proton Events at the Air Force Global Weather Central's Space Environmental Forecasting Facility," *Proceedings of the 1978 Symposium on the Effect of Ionosphere on Space and Terrestrial Systems* (Arlington, VA), edited by John M. Goodman, U.S. Government Printing Office, Washington, DC, 1978, pp. 393–400.

[5]Smart, D. F., and Shea, M. A., "PPS76—A Computerized 'Event Mode' Solar Proton Forecasting Technique," *Solar Terrestrial Prediction Proceedings*, edited by R. F. Donnelly, Vol. 1, National Oceanic and Atmospheric Administration/Environmental Research Lab., U.S. Dept. of Commerce, 1979, pp. 406–423.

[6]Smart, D. F., and Shea, M. A., "Galactic Cosmic Radiation and Solar Energetic Particles," *The Handbook of Geophysics and the Space Environment*, edited by A. S. Jursa, U.S. Air Force Geophysics Lab., Bedford, MA, 1985, Chap. 6, pp. 1–29.

[7]Heckman, G. R., Kunches, J. M., and Allen, J. H., "Prediction and Evaluation of Solar Particle Events Based on Precursor Information," *Advances in Space Research*, Vol. 12, Nos. 2–3 , 1992, pp. 313–320.

[8]Smart, D. F., and Shea, M. A., "Predicting and Modeling Solar Flare Generated Proton Fluxes in the Inner Heliosphere," *Biological Effects and Physics of Solar and Galactic Cosmic Radiation, Part B; Proceedings of a NATO Advanced Study, Institute on Biological Effects and Physics of Solar and Galactic Cosmic Radiation* (Algarve, Portugal, 1991), A95-81431, NATO ASI Series A, Life Sciences Vol. 243B, Plenum, New York, 1993, pp. 101–117.

[9]Smart, D. F., and Shea, M. A., "Modeling the Time Intensity Profile of Solar Flare Generated Particle Fluxes in the Inner Heliosphere," *Advances in Space Research*, Vol. 12, Nos. 2, 3, 1992, pp. 303–312.

[10]Acton, C. H., Jr., "Using the Spice System to Help Plan and Interpret Space Science Observations," *Proceedings of SPACEOPS 92: The Second International Symposium on Ground Data Systems for Mission Operations*, Jet Propulsion Lab., California Inst. of Technology, Pasadena, CA, 1993, pp. 781–786.

[11]Parker, E. N., *Interplanetary Dynamical Processes*, Monographs and Texts in Physics and Astronomy, edited by R. E. Marshak, Vol. 8, Interscience, New York, 1963, Chap. 10, pp. 131–150.

[12]Beeck, J., Mason, G. M., Hamilton, D. C., Wibberenz, G., Kunow, H., Hovestadt, D., and Klecker, B., "A Multispacecraft Study of the Injection and Transport of Solar Energetic Particles," *Astrophysical Journal*, Vol. 322, No. 2, 1987, pp. 1052–1072.

[13]Shea, M. A., and Smart, D. F., "History of Energetic Solar Particles for the Past Three Solar Cycles Including Cycle 22 Update," *Biological Effects and Physics of Solar and Galactic Cosmic Radiation*, Part B, edited by C. E. Swenberg, G. Horneck, and E. G. Stassinopoulos, Plenum, New York, 1993, pp. 37–71.

[14]Sarris, E. T., Krimigis, S. M., "Interplanetary Energetic Particle Observations of the March 1989 Events," *Max '91, Workshop 2: Developments in Observations and Theory for Solar Cycle 22*, NASA Goddard Space Flight Center, 1991, pp. 246, 247.